ACS OMEGA

Open Access

http://pubs.acs.org/journal/acsodf

Article

Quantitative Effects of the Loop Region on Topology, Thermodynamics, and Cation Binding of DNA G-quadruplexes

Minori Nakata, Naoki Kosaka, Keiko Kawauchi, and Daisuke Miyoshi*

Cite This: *ACS Omega* 2024, 9, 35028−35036

Read Online

ACCESS | Metrics & More | Article Recommendations | Supporting Information

ABSTRACT: The thermal stability of G-quadruplexes is important for their biological roles. G-quadruplexes are stable in the presence of cations such as K^+ and Na^+ because these cations coordinate in the G-quartet of four guanine bases. It is well known that the number of G-quartets and the configuration of the guanine bases affect the binding affinity of the cation. Recently, structures formed in the loop regions connecting the guanine stretches have attracted significant attention, because the loop region affects G-quadruplex properties, such as topology, thermal stability, and interactions with proteins and small molecules. Considering these effects, the loop region can also affect the binding affinity of the cations. Here, we designed a series of G-quadruplex-forming DNA sequences that contain a hairpin in a loop region and investigated the effects of the sequence and structure of the loop region on the cation binding affinity as well as the thermal stability of the G-quadruplex as a whole. First, structural analysis of the DNA sequences showed that the hairpin at the loop plays a key role in determining G4 topology (strand orientation). Second, in the case of the G-quadruplexes with the hairpin-forming loop region, it was found that a longer loop length led to a higher thermodynamic stability of the G-quadruplex as well as higher cation binding affinity. In contrast, an unstructured loop region did not lead to such effects. Interestingly, the cation binding affinity was correlated to the thermodynamic stability of the hairpin structure at the loop region. It was quantitatively demonstrated that the stable loop region stabilized the whole G-quadruplex structure, which induced higher cation binding affinity. These systematic and quantitative results showed that the loop region is one of the determinants of cation binding and expanded the possibilities of drug development targeting G4s by stabilizing the loop region.

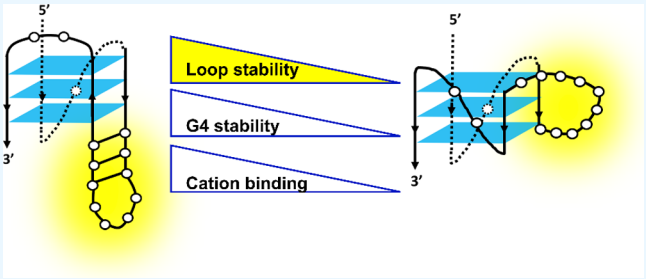

1. INTRODUCTION

Guanine-rich DNA sequences can fold into a G-quadruplex (G4), which is a four-stranded helical structure built from multiple G-quartets with Hoogsteen base pairs between the four guanine bases.[1,2] In the human genome, G4-forming sequences have been identified at telomeres and other biologically important regions such as promoters and introns of various genes.[3−8] In these regions, DNA G4 controls biological events such as telomerase elongation,[9] replication,[10] and transcription.[11,12] Moreover, DNA G4 participates in the onset mechanisms of a variety of diseases.[13−15] Thus, G4s are attractive drug targets for cancer,[16,17] neurodegenerative diseases,[18] and virus infections.[19,20] Since there is a relationship between G4 thermodynamics and the inhibitory effects on enzymes related to gene expression,[11,16,21] factors affecting the thermodynamics of G4s have been extensively studied.[22−26]

Metal cations are well-known critical factors for forming and stabilizing G4s *in vitro* and *in vivo*.[6] Cations mainly bind to the O6 atoms of the guanines, which are located in the center cavity of the G-quartet. Thus, the ionic radius of the cation has been considered to be a key factor in determining the binding affinity of the cation with DNA G4.[25,27] Furthermore, it was shown that G4 is stabilized by dehydration from the cations upon binding to the G-quartets.[27] These two features of cations, the ionic radius and the dehydration energy, were reported to be almost equally important for the binding affinity of cations with G4.[28] Glycosidic bond orientation also affects the behavior of cations: *syn* glycosidic bond orientation penalizes the release of K^+, which results in asymmetrical cation movements though the two terminals of G4s.[29] Zaccaria et al. revealed that the cation is not needed to reduce repulsion between the oxygen atoms but rather provides additional stability of the G-quadruplex by electrostatic and donor−acceptor interactions between the oxygens and the cations.[28]

Oganesian et al. reported that a *Tetrahymena* telomeric DNA G4 sequence suppresses telomerase elongation by forming a stable G4 in the presence of K^+ or Na^+, and the suppression efficiency depends on the coexisting cation species.[30] More-

Received: May 28, 2024
Revised: July 16, 2024
Accepted: July 17, 2024
Published: July 30, 2024

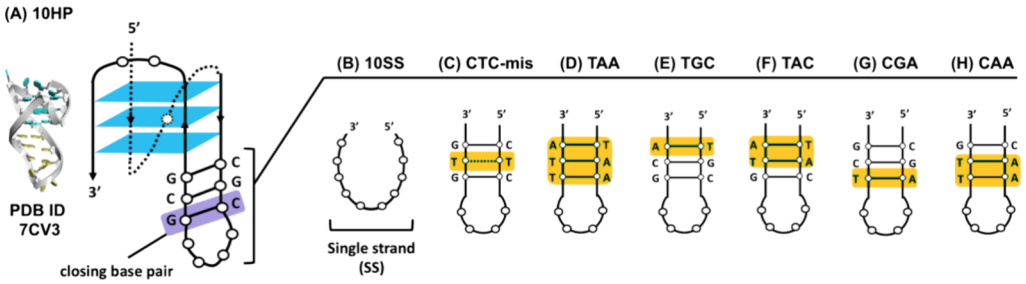

Figure 1. (A) G4 structure (PDB ID: 7CV3) of 10HP. 10HP includes a hairpin with three GC base pairs at the second loop region from the 5′ end. (B–H) Loop sequences of DNA oligonucleotides designed based on 10HP. (B) 10SS: no structure is formed. (C) CTC-mis: one GC base pair was replaced by one TT mismatched base pair. (D) TAA: three GC base pairs were replaced by three AT base pairs. (E) TGC: one GC base pair was replaced by one AT base pair on the distal side from the loop. (F) TAC: two GC base pairs were replaced by two AT base pairs on the distal side from the loop. (G) CGA: one GC base pair was replaced by one AT base pair on the proximal side from the loop. (H) CAA: two GC base pairs were replaced by two AT base pairs on the proximal side from the loop. Mutation sites are highlighted in yellow.

Table 1. Sequences of DNA Oligonucleotides Used in This Study[a]

Abbreviation	Sequence (5' to 3')[a]		
10SS	GCGGGAGGG	AGCGAATATA	GGGTCGGG
10HP	GCGGGAGGG	CGCGCCAGCG	GGGTCGGG
CTC-mis	GCGGGAGGG	CTCGCCAGTG	GGGTCGGG
TAA	GCGGGAGGG	TAAGCCATTA	GGGTCGGG
TGC	GCGGGAGGG	TGCGCCAGCA	GGGTCGGG
TAC	GCGGGAGGG	TACGCCAGTA	GGGTCGGG
CGA	GCGGGAGGG	CGAGCCATCG	GGGTCGGG
CAA	GCGGGAGGG	CAAGCCATTG	GGGTCGGG

[a]Base pairs in the hairpin stem of the second loop region are underlined.

over, the thermal stability of G4s, which is dependent on coexisting cation species, is critical not only for telomerase inhibition but also for other regulatory roles of G4s.[11,21,31] These phenomena clearly demonstrate that cation binding is one of the determinants for forming and stabilizing G4s[22,23,25,27,32] to play their biological roles.

Recently, the loop region of G4 has attracted attention as a structural element for controlling topology,[33,34] thermal stability,[33,35] folding kinetics,[36] and interactions with small molecules and proteins of G4.[37−39] Therefore, it is considered that the loop regions further affect the cation binding. In fact, Podbevšek et al. showed that the cation exchange rate constant for an unimolecular G4, d$[G_4(T_4G_4)_3]$ containing a single diagonal loop, is 80 times slower than that for a bimolecular G4 d$(G_4T_4G_4)$ composed of two diagonal loops.[40] It was also reported that the longer the loop length of G4, the lower the binding affinity of K^+ to G4s.[41] These results strongly suggest that one should consider not only the G-quartet but also the loop region to reveal the determinants of the cation binding affinity with G4s. However, the roles of the loop region in binding of the cation to G4 still remain unclear.

In this study, we investigated the effects of structures formed in a loop region of G4 on the cation binding affinity. We utilized DNA G4, in which one of the loop regions folds into a hairpin loop structure.[42] (Here, we refer to "the hairpin loop structure" formed at the loop region as a "hairpin" to avoid ambiguity.) We designed G4s that have a hairpin at the second loop with various thermal stabilities. Structural analysis of the DNA sequences showed that the hairpin at the loop forces a hybrid G4. Thermodynamic analysis revealed that the more stable hairpin leads to the higher stability of the overall G4 and the higher binding affinity with K^+. These systematic results demonstrate that the loop region is one of the determinants of thermodynamics and cation binding affinity of G4, thus expanding the possibilities of drug development targeting G4 by targeting the loop region or stabilizing G4s with long loop regions.

2. RESULTS AND DISCUSSION

2.1. Sequence Design of G4s Having Various Hairpin Structures in the Loop Region. Phan and his colleagues reported a hybrid type G4 (with one of the four G-stretch regions in the opposite direction to the other three), containing a hairpin structure at the second loop region from the 5′ end (Figure 1A and Table 1).[42] This sequence is derived from the PIM1 gene, which is overexpressed in triple-negative breast cancer cells,[43] hematopoietic cancer cells,[44] and prostate cancer cells.[45] The hairpin is composed of a stem with three G-C base pairs and a four-base loop (5′-GCCA-3′). To systematically investigate the effects of the loop structure on the thermal stability of the overall G4 structure and the cation binding affinity, a series of G4s were designed as follows (Figure 1B–H and Table 1). 10SS: without hairpin; CTC-mis: one TT mismatched base pair in the stem; TAA: three AT base pairs in the stem; TGC: one AT base pair at the distal side from the loop; TAC: two AT base pairs at the distal side from the loop; CGA: one AT base pair at the proximal side from the loop; CAA: two AT base pairs at the proximal side from the loop. These DNA sequences have the same length of the loop region, and only the composition of nucleobases is different.

2.2. Structural Analysis of G4s. The structures of the designed DNA oligonucleotides were studied by circular dichroism (CD). Figure 2A shows the CD spectra of 10 μM

https://doi.org/10.1021/acsomega.4c05008
ACS Omega 2024, 9, 35028−35036

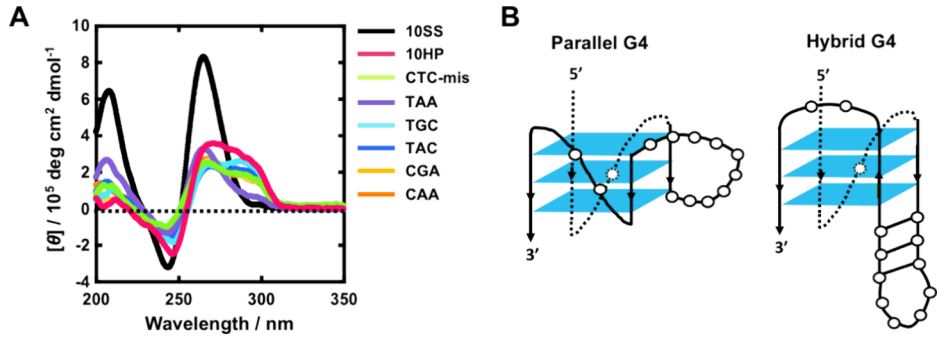

Figure 2. (A) CD spectra of 10 μM DNA oligonucleotides in a buffer containing 100 mM KCl, 10 mM LiH_2PO_4, and 1 mM Li_2EDTA (pH 7.0) at 25 °C. (B) Schematic structures of (left) parallel G4 and (right) hybrid G4.

DNA oligonucleotides in a buffer containing 100 mM KCl, 10 mM LiH_2PO_4 (pH 7.0), and 1 mM Li_2EDTA at 25 °C. The CD spectrum of 10SS (black color) showed positive and negative peaks around 265 and 240 nm, respectively, indicating a parallel G4 (left, Figure 2B).[46] Since a loop with a single nucleotide strongly promotes a parallel topology irrespective of the length and composition of other intervening sequences,[33] the parallel G4 of 10SS is induced by the single adenine nucleotide at the first (5′ side) loop. The CD spectrum of 10HP (red) showed positive peaks around 295 and 265 nm, indicating a hybrid G4[46] (right, Figure 2B), confirming the hybrid G4 reported by NMR spectroscopy.[42] Similar to 10HP, other DNAs (CTC-mis, TGC, TAC, CGA, and CAA) showed positive peaks around 295 and 265 nm, indicating hybrid G4 structures, although there should be small differences in their structures. Comparing 10SS and others, it is reasonable to consider that the oligonucleotides with the hairpin structure at the second loop force the formation of the hybrid G4, even with the single-nucleotide loop at the 5′ side. These hairpin effects may be useful to lock the G4 topology, by which protein recognition is altered. In addition, TAA shows a CD spectrum similar to that of 10SS, indicating a parallel G4 formation. We will discuss this point later with a more detail analysis.

To confirm the structure of G4s with the series of loop sequences, we carried out nondenaturing polyacrylamide gel electrophoresis (PAGE) (Figure S1). All sequences showed the main single band, although some of the sequences (10HP and CGA) showed a very faint band, migrating slightly faster than the main band. Considering that 10HP was confirmed by NMR to form the hybrid G4,[42] these results suggest that all sequences mainly fold to form a single monomeric G4 structure. The difference in the migrations can be attributed to variations in the loop region.[47,48] In addition, 10SS, TAA, and CAA showed minor bands migrating very slowly. These bands indicate that there are high-order structures, such as multimeric G4s and G-wire,[49,50] although it is difficult to determine the structure. We further performed CD melting experiments (Figure S2) and SVD analysis of the CD spectra at different temperatures to identify the major structure by the use of KinTek Explorer (see Experimental Details). Figure S3A shows the most major and second major components of the 10 HP CD spectra. The most major component (SV = 66) has the main positive peak around 260 nm with a shoulder around 295 nm, showing that the main component is a hybrid G4.[46] The second major component has the main peak around 295 nm, suggesting that this component corresponds to an antiparallel G4.[46] In the case of 10SS (Figure S3B), the most major component shows a parallel G4, whereas the second one does not show any significant structure. The most major component of CTC-mis (Figure S3C), TGC (Figure S3E), TAC (Figure S3F), CGA (Figure S3G), and CAA (Figure S3H) was similar to 10HP, indicating a hybrid G4. On the other hand, the most major component of TAA (Figure S3D) was similar to 10SS, suggesting a parallel G4. Except for TGC, the second major component was an antiparallel G4. Note that the SV value of most of the major components was much larger than that of the second major components, suggesting that all DNA sequences fold to form the dominant structure. These SVD analyses are consistent with the structural characterization based on CD spectra shown in Figure 2. The difference between TAA and other HP G4s may lead to a different effect of hairpin on the thermal stability and the cation binding affinity of G4s as we discuss later with the thermodynamic parameters. Figure S4 shows the melting curves of the most and second major components. Noteworthily, the melting curves of the major components of all sequences were almost the same with the UV melting curve tranced at 295 nm (Figure S5), suggesting that the UV melting curves reflect the most major components. From these considerations, we assumed a two-state transition between a random coil and a hybrid G4 for the HP DNAs, except TAA, although a minor antiparallel G4, which denatured at lower temperature, coexists. In the case of 10SS and TAA, it is possible to assume a two-state transition between a random coil and a parallel G4.

Similar to the hybrid G4 of HP DNAs here, it was shown that a DNA oligonucleotide derived from an hTERT formed an antiparallel G4 through the hairpin formation at the second loop.[51] These results suggest that the hairpin at the loop region significantly affects the G4 topology by limiting the combinations of Hoogsteen base pairs formed among guanine residues. Kinetic studies of the G4 folding also support the importance of the hairpin formation: it has been proposed that a G4 is formed through a G-hairpin formation, in which guanine−guanine base pairs are produced.[52,53] The hybrid G4 and the parallel G4 of 10HP and 10SS, respectively, may support the formation of G-hairpins following the hairpin formation at the loop region, which determines the G4 topology. Furthermore, it has been reported that bases of a hairpin in the central lateral loop can interact with the neighboring G-quartet through $\pi-\pi$ stacking in the case of antiparallel and hybrid G4s, but not in the case of a parallel one,[34,35,42] indicating that the hairpin structure at the lateral loop can also stabilize the whole G4. From these results and considerations, it is possible to conclude that the hairpin structure in 10HP guides the hybrid G4 topology, and this

https://doi.org/10.1021/acsomega.4c05008
ACS Omega 2024, 9, 35028−35036

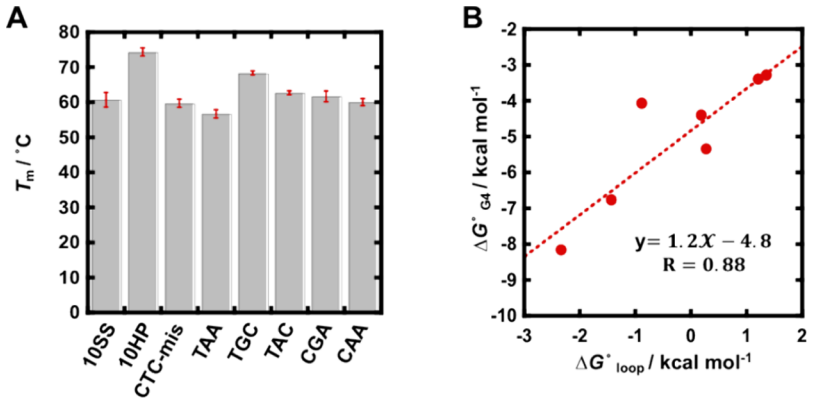

Figure 3. (A) Thermal melting temperature of 10 μM DNA oligonucleotides in the KCl buffer. (B) Plots of ΔG°_{G4} versus ΔG°_{loop} in the buffer at 25 °C. ΔG°_{loop} is the free energy change of the hairpin evaluated with *m*-fold (see the main text).

Table 2. Thermodynamic Parameters for DNA Structures at 25 °C[a]

abbreviation	ΔG°[b,c] (kcal mol^{-1})	ΔH° (kcal mol^{-1})	$T\Delta S^\circ$ (kcal mol^{-1})	T_m (°C)	ΔG°_{loop}[d] (kcal mol^{-1})
10SS	−5.0 ± 0.9	−46.3 ± 6.2	−41.4 ± 5.3	61 ± 2.1	N.D.[e]
10HP	−8.4 ± 0.2	−59.1 ± 1.6	−50.7 ± 1.5	74 ± 1.2	−2.3
CTC-mis	−3.9 ± 0.5	−36.6 ± 4.5	−32.7 ± 3.9	60 ± 1.2	1.4
TAA	−3.8 ± 0.4	−39.3 ± 2.7	−35.5 ± 2.3	57 ± 1.2	1.2
TGC	−7.0 ± 0.3	−55.2 ± 2.8	−48.2 ± 2.5	68 ± 0.6	−1.4
TAC	−6.0 ± 0.7	−53.7 ± 4.8	−47.6 ± 4.1	63 ± 0.6	0.3
CGA	−4.7 ± 0.6	−42.8 ± 4.0	−38.0 ± 3.4	62 ± 1.6	−0.9
CAA	−4.5 ± 0.1	−42.6 ± 1.5	−38.1 ± 1.4	60 ± 1.0	0.2

[a]All experiments were carried out in a buffer containing 100 mM KCl, 10 mM LiH_2PO_4, and 1 mM Li_2EDTA (pH 7.0). [b]Values of ΔG°, ΔH°, $T\Delta S^\circ$, and T_m reported are averages ± standard deviations for the three experiments. [c]The melting temperature was determined at a strand concentration of 10 μM. [d]ΔG°_{loop} is the free energy change of the hairpin evaluated with *m*-fold. [e]ΔG°_{loop} of 10SS could not be calculated by *m*-fold, because no structure was identified.

compulsion is stronger than that derived from the single nucleotide loop that promotes the parallel G4 as observed for 10SS. Thermodynamic effects of the hairpin structure at the loop will be discussed next.

2.3. Thermodynamic Analysis of G4s. To investigate the effects of the loop structure on the G4 thermodynamics, we performed UV-melting analysis monitored at 295 nm[54] in the 100 mM KCl buffer (Figure S5) and the melting temperature, T_m, values were evaluated (Figure 3A). The thermodynamic parameters for the G4 folding of the oligonucleotides were further evaluated with a curve fitting procedure for the melting curves with an assumption of a two-state transition between a random coil and a G4,[55] and they are listed in Table 2. The values of T_m for 10SS and 10HP were 61 ± 2.1 and 74 ± 1.2 °C, respectively. The values of ΔG°_{25} for these DNAs were −5.0 ± 0.9 and −8.4 ± 0.2 kcal/mol, respectively. Comparing 10SS and 10HP, it was found that the hairpin structure in the loop stabilized the G4 by 13 °C and 3.4 kcal/mol in the values of T_m and ΔG°_{25}, respectively. This stabilization is provided by the thermodynamically favorable change in ΔH° (from −46.3 ± 6.2 to −59.1 ± 1.6 kcal/mol), which exceeds the unfavorable change in $T\Delta S^\circ_{25}$ (from −41.4 ± 5.3 to −50.7 ± 1.5 kcal/mol), showing that the hairpin structure at the loop stabilizes the G4 with some additional interactions, such as hydrogen bonding and stacking interactions. However, it should be noted that the 10SS and 10HP structures are the parallel G4 and the hybrid G4, respectively. Therefore, it is more suitable to compare the parameters of the hybrid G4s excluding 10SS.

The most unstable G4 was CTC-mis (ΔG°_{25} = −3.9 ± 0.5 kcal/mol). This has one T-T mismatch in the hairpin stem, which may dissociate the hairpin structure. Interestingly, ΔH° and $T\Delta S^\circ$ for TGC and TAC were smaller than those for CGA and CAA despite having the same components in the hairpin stem, differing only in the permutation. As shown in Figure 1 and Table 1, CGA and CAA contain a hairpin that has one or two AT base pairs at the proximal side from the single strand loop. TGC and TAC contain a hairpin that has one or two AT base pairs on the distal side from the loop. It is significant that one closing base pair of the hairpin contributes to a more favorable ΔH°. It is well known that the thermal stability of DNA and RNA hairpins depends on the closing base pair,[56−58] which is the nearest neighbor one next to the nonbase paired loop region (see Figure 1A). For example, ΔH° and $T\Delta S^\circ$ for the DNA hairpin loop of d(ggacGCACgtcc) (where capital and small letters show the hairpin region and the stem region, respectively, and bold font shows the closing base pair) are smaller than those for d(ggaaGCACttcc) by about 12 and 9 kcal/mol, respectively.[57] This result showed that the GC base pair is more favorable as the closing base pair than the AT one.[57,59,60] These previous results are consistent with those obtained here. Along the same line, 10HP is stabilized due to the favorable enthalpy contribution of the GC closing base pair.

Figure 3B shows the relationship between ΔG°_{G4} (ΔG° value of G4) and ΔG°_{loop} (ΔG° value of the hairpin). We used the thermodynamic parameters of the hairpin formation evaluated with *m*-fold,[61] because some of the loop sequences did not show a clear melting curve at 260 nm of UV. It was found that the smaller the value of ΔG°_{loop}, the smaller the value of ΔG°_{G4}, demonstrating that there is a relationship

https://doi.org/10.1021/acsomega.4c05008
ACS Omega 2024, 9, 35028−35036

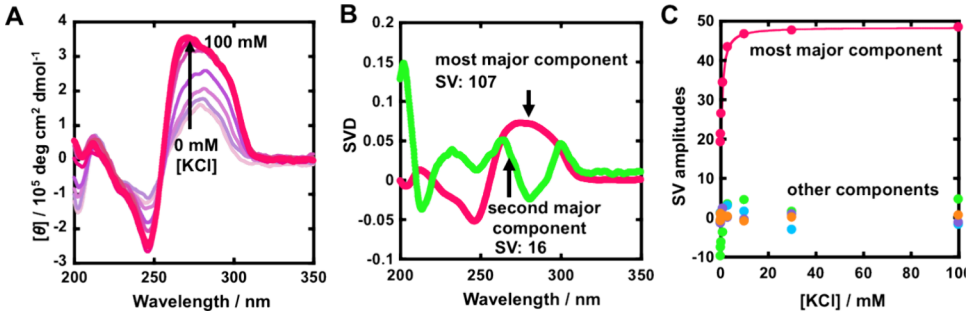

Figure 4. (A) CD spectra of 10 μM 10HP in the presence of various concentrations (0, 0.1, 0.3, 1, 3, 10, 30, and 100 mM) of KCl in buffer containing 10 mM LiH_2PO_4 and 1 mM Li_2EDTA (pH 7.0) at 25 °C. (B) Results of SVD analysis of the CD spectra. Most (red) and second (green) major SVD spectra (components) derived from the CD spectra with different KCl concentrations. (C) Plots of the SVD amplitude (magenta: most major component; green: second major component) of 10HP versus KCl concentration. Other colors, violet, orange, and blue, are the third, fourth, and fifth major components, respectively.

between the thermal stability of the hairpin structure at the loop region and the thermal stability of the G4 structure. Previously, it was reported that a hairpin at the central lateral loop region increases the thermal stability of the overall G4 structure,[34,35] whereas the hairpin at the propeller loop does not.[34,35] As mentioned above, some bases in the hairpin can stack onto G-quartets in the case of a lateral loop.[34,35] Similarly, the structure of 10HP may have a stacking interaction between the hairpin stem base pair and the neighboring G-quartet.[42] Combined with enthalpic stabilization (Table 2), it is reasonable to conclude that G4 is stabilized by stacking with a thermodynamically stable hairpin. This finding may be useful for designing G4-forming sequences with higher thermal stability toward more efficient gene regulation and development of G4-forming functional molecules such as aptamers and biosensor.

2.4. Cation Binding with G4. The above results demonstrated that the loop region alters the strand orientation and the thermodynamics of the entire G4. Because of the importance of the loop region, we further attempted to study the effects of the loop structure on the cation binding affinity of G4. The values of K_{half}, the K^+ concentration required to fold half of the G4, were evaluated from K^+ titration experiments. Figure 4A shows CD spectra of 10HP with various concentrations of K^+ (0, 0.1, 0.3, 1, 3, 10, 30, and 100 mM). We carried out SVD analysis of the CD spectra with different K^+ concentrations.

Figure 4B shows SVD spectra of the most and second major components of 10HP during the K^+ titration. The CD spectrum of the most major component (SV = 107) showed two positive peaks around 265 and 295 nm, which is the typical for a hybrid G4.[33,62] The second major component (SV = 16) showed positive and negative peaks around at 300 and 280 nm, respectively. Chaires group reported a similar spectrum, which is derived from diagonal and lateral loops.[46] Other minor components showed no significant peak (data not shown). The most major component, corresponding to the hybrid G4, was amplified with higher K^+ concentration, whereas the second major one was not (Figure 4C). These results confirm that the hybrid G4 of 10HP is mainly induced by the addition of K^+. Similar results (SVD spectra and SV) were found in other sequences (10SS, CTC-mis, TAA, TGC, TAC, CGA, and CAA). CD spectra for K^+ titration are shown in Figure S6. The most and second major components are shown in Figure S7. Note that the most major component of TAA was similar to 10SS, indicating a parallel G4. These results are consistent with the SVD analysis for CD melting (Figure S3).

We calculated the values of K_{half} and n from the SVD amplitude vs K^+ concentration plot of the most significant component by a curve fitting procedure using eq 1 (Figure 4C and Figure S8), and they are summarized in Table 3. It was

Table 3. Binding Affinity of G4 Evaluated from SVD Analysis of G4s with K^+[a]

abbreviation	K_{half}[b] (mM)	n[b]	$\Delta G°_{K+}$(kcal mol^{-1})
10SS	5.8 ± 0.3	1.6 ± 0.1	−2.7
10HP	0.9 ± 0.1	1.2 ± 0.1	−3.3
CTC-mis	3.0 ± 1.1	1.4 ± 0.6	−2.9
TAA	3.1 ± 0.4	2.0 ± 0.4	−4.1
TGC	0.8 ± 0.1	1.1 ± 0.1	−3.1
TAC	1.4 ± 0.2	1.2 ± 0.1	−3.0
CGA	4.9 ± 0.7	1.1 ± 0.1	−2.0
CAA	1.5 ± 0.03	1.2 ± 0.03	−3.0

[a]The values of K_{half} and n were calculated from the plots shown in Figure S7. Two significant components were chosen based on the values of SV (Figure S6). These values indicate the significance of the component. [b]Error values of K_{half} and n are calculated by a curve fitting of SV amplitude by KinTek Explorer.

shown that the K_{half} value for 10HP at 25 °C (0.9 ± 0.1 mM) was about 6-fold smaller than that for 10SS (5.8 ± 0.3 mM), indicating that the hairpin at the loop region contributes to the binding affinity with K^+. The K_{half} values for other G4s (CTC-mis, TAA, TGC, TAC, CGA, and CAA) fell between those of 10SS and 10HP. Figure 5A shows the correlation between $\Delta G°_{K^+}$ (the free energy change for the K^+ binding) and $\Delta G°_{loop}$ (free energy change for the hairpin formation) at 25 °C. The value of $\Delta G°_{K^+}$ was determined from the K_{half} values (Table 3) using eq 2. To generalize the relationship between the $\Delta G°_{K^+}$ and $\Delta G°_{loop}$, we added data points of three other G4s, 8HP, 14HP, and 20HP, which have hairpins with 8, 14, and 20 nucleotides, respectively. Their nucleotide sequences are listed in Table S1, and the binding parameters with K^+ were evaluated as shown in Figure S9 and summarized in Table S2. Except for TAA (highlighted in white color), it was found that the lower the value of $\Delta G°_{loop}$, the lower the value of $\Delta G°_{K^+}$ (Figure 5A). This relationship suggests that the stabilization of the loop region enhances the cation binding affinity of G4. Since we showed that the hairpin structure at the loop region leads to the stabilization of the G4 structure

https://doi.org/10.1021/acsomega.4c05008
ACS Omega 2024, 9, 35028−35036

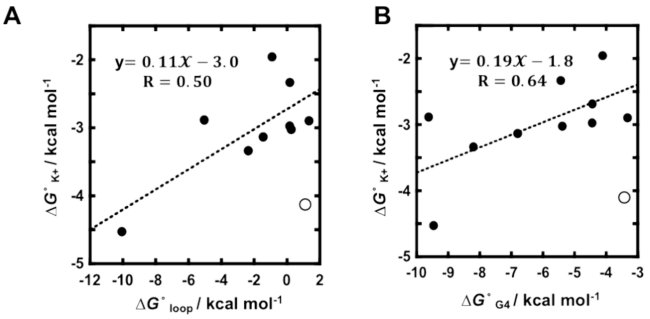

Figure 5. (A) Plots of $\Delta G^{\circ}_{K^+}$ versus ΔG°_{loop} in the KCl buffer. (B) Plots of ΔG°_{G4} versus $\Delta G^{\circ}_{K^+}$. The values of ΔG°_{loop} were calculated using the *m*-fold application under the condition with 100 mM KCl at 25 °C (see the main text). The equations are the results of the linear fitting of the plots without TAA shown as a white circle (see the main text).

(Figure 3B), it is considerable that the thermal stability of the overall G4 structure has a relationship with the cation binding affinity. As shown in Figure 5B, the lower the values of ΔG°_{G4}, the lower the values of $\Delta G^{\circ}_{K^+}$, suggesting that the more stable G4 structure has stronger binding affinity with K^+. These results show the importance of the hairpin at the loop to determine cation binding affinity. Although it is unknown how the G4 stability affects the cation binding affinity of G4, it is considerable that the hairpin indirectly affects the cation binding to the G4 via the thermodynamic stability of G4, which is affected by the hairpin thermodynamics. Further structural study is required to confirm the hairpin formation and the whole G4 in more detail. Notably, the data shown in a white circle correspond to TAA, which forms a parallel G4 as we discussed above (Figure 2 and Figure S3). The deviation of TAA from the relationship should be due to the difference in the topology, further supporting the importance of the hairpin in the cation binding affinity. Although the correlation between the thermodynamic stability of G4s and their cation binding affinity may not be surprising, to the best of our knowledge, there is no study showing this relationship in a quantitative manner. The linear relationship between ΔG°_{loop} and $\Delta G^{\circ}_{K^+}$ showed that the free energy change of the K^+ binding is −3.0 kcal/mol when there is no loop contribution. In the same way, the free energy change of the K^+ binding is −1.8 kcal/mol when the thermodynamic stability of a G4 is zero. In addition, to test the importance of the hairpin for the relationship, we further added some other naturally occurring G4 sequences (VEGF, TeloT, TeloTT, and RET), which do not possess the hairpin structure in the loop region. See Tables S2 and S3 for the K^+ binding parameters and nucleotide sequences, respectively. The K^+ titration results and their SVD analyses are shown in Figure S10. Figure S11 shows the plot of ΔG°_{G4} vs $\Delta G^{\circ}_{K^+}$ for these naturally occurring G4s (red color) as well as the HP (black color) and TAA (white color) G4s. Interestingly, it was found that the stability−cation affinity relationship of G4s was not observed for G4s without a hairpin in the loop. These results confirm the importance of the hairpin at the loop to determine the cation binding affinity of G4. A similar trend was observed in previous reports. For example, it was reported that the binding affinity of G4 with K^+ having a short loop region is higher than that of G4 having a long loop region.[41] G4s with shorter loops generally possess higher thermal stability.[24,33,63] These results are consistent with our findings for the stability−cation affinity relationship of G4, although further studies are required for the mechanism. To date, the binding affinity between G4 and cations has been studied from the viewpoint of their binding with G-quartet regions, because guanine and O6 atoms are the binding sites. We quantitatively and systematically revealed that the thermal stability of the loop region is also one of the determinants of the G4 topology, thermodynamic stability, and cation binding affinity.

3. CONCLUSIONS

In this study, we quantitatively and systematically investigated the effects of the loop structure on the topology, thermodynamic stability, and cation binding affinity of G4s. We designed various G4 sequences that formed hairpins in the second loop region. Structural analysis showed that the G4 topology was altered depending on the loop structure, even though the nucleotide length of the loop was the same. The G4s with the 10 nucleotide-length hairpin structure at the second loop region (10HP, CTC-mis, , TGC, TAC, CGA, and CAA) folded into the hybrid G4 form, guided by the hairpin, in contrast to the parallel G4 of 10SS and TAA in which no hairpin structure was formed. The relationship between the thermodynamic stability of the hairpin in the loop region and that of the overall G4 structure showed that the more stable hairpin increased the stability of the overall G4 structure. These loop effects may be useful for predicting the strand orientation and thermodynamics of the G4-forming sequences. Finally, it was shown that the G4s stabilized by the hairpin at the loop region bind to K^+ with high affinity. This relationship suggests that the structured loop accelerates the formation of a stable G4 that requires a lower K^+ concentration for the folding. The results obtained here expand the possibilities of drug development for G4s by targeting the loop region or stabilizing G4s with long loop regions, which has not received much attention to date. This strategy is also useful for designing G4-forming robust functional molecules, such as aptamers and biosensors, that can maintain stable structures in the cell, where many environmental factors, including cation concentration, change depending on cell cycle and condition.

4. EXPERIMENTAL DETAILS

4.1. Sample Preparation. All DNA oligonucleotides were purchased from Sigma-Aldrich Japan K. K. (Tokyo, Japan). Each oligonucleotide concentration was determined by the absorbance at 260 nm. Extinction coefficients for single-stranded DNA were calculated from the mono- and dinucleotide data using the nearest-neighbor approximation model.[64] The absorbance was measured using a UV-1800 spectrophotometer (Shimadzu, Kyoto, Japan). Chemical reagents were purchased from FUJIFILM Wako Pure Chemical Co. (Osaka, Japan) and Tokyo Chemical Industry Co., Ltd. (Tokyo, Japan). All of the reagents were used without further purification.

4.2. Circular Dichroism Measurements. Circular dichroism (CD) measurements were performed by using a Jasco CD J1500 spectropolarimeter (Jasco Co., Ltd., Tokyo, Japan), and data were analyzed with Jasco Spectra Manager Suite software. DNA oligonucleotides were prepared at a concentration of 10 μM. CD spectra were acquired in the wavelength range of 200−350 nm in a cuvette with a path length of 0.1 cm. CD spectra are an average of 2 scans with a response time of 4 s/

https://doi.org/10.1021/acsomega.4c05008
ACS Omega 2024, 9, 35028−35036

nm. Before measurement, each sample was heated to 90 °C for 5 min and gently cooled to 25 °C at a rate of 0.5 °C/min.

CD titration experiments on G4s were performed with 10 μM oligonucleotide at 25 °C in the presence of various concentrations (0, 0.1, 0.3, 1, 3, 10, 30, and 100 mM) of KCl in a buffer containing 10 mM LiH_2PO_4 (pH 7.0) and 1 mM Li_2EDTA.

4.3. Singular Value Decomposition Analysis.

$$\text{SV amp.} = (\text{SV amp.}_{\max} - \text{SV amp.}_{\min})\left(\frac{[K^+]^n}{[K^+]^n + [K_{\text{half}}]^n}\right) + \text{SV amp.}_{\min} \quad (1)$$

For the singular value decomposition (SVD) analysis, the CD spectra with different KCl concentrations were arranged in the text file. SVD decomposition was carried out using the software KinTek Explorer (KinTek Corp., Pennsylvania, U.S.A.). The mathematical details of the SVD analysis have been described elsewhere.[65] The KinTek program abstracts five components from the imported data.[66] The significant spectra were determined by evaluating a statistical parameter, the relative magnitude of the singular values (SVs).[46] For example, SV = 100 for one component, while SV = 10 for the second component, indicating a greater significance for the former one. Moreover, the KinTek program shows the plots of SV amplitude of respective components scaled by their SV versus K^+ concentration. The plots of SV amplitude vs K^+ concentration were fitted with eq 1 using KaleidaGraph (Synergy software, Pennsylvania, U.S.A.) to evaluate the value of K_{half},[67,68] the K^+ concentration required to fold half the DNA, where SV amp. is the SV amplitude of the component with different concentrations of K^+. $\text{SV amp.}_{\max}$ and $\text{SV amp.}_{\min}$ are the maximum and minimum SV amplitudes, respectively, in the titration experiment. The n shows the Hill coefficient value.

The free energy change of the binding of K^+ to G4 (ΔG°_{K+}) was calculated from the value of K_{half} using eq 2,

$$\Delta G_\circ^{K+} = -nRT\ln\left(\frac{[K^+]}{[K_{\text{half}}]}\right) \quad (2)$$

where R is the gas constant and T is the temperature in K.

4.4. Thermodynamic Analysis. UV melting curves for each oligonucleotide were measured at 295 nm by using a UV-1800 spectrophotometer (Shimadzu Co., Ltd., Kyoto, Japan) with a temperature controller. All experiments were carried out in a buffer containing 100 mM KCl, 10 mM LiH_2PO_4 (pH 7.0), and 1 mM Li_2EDTA. The thermodynamic parameters were calculated from the melting curves by a curve fitting procedure as described previously with an assumption of a two-state transition.[69,70]

■ ASSOCIATED CONTENT

Data Availability Statement

All data generated or analyzed during this study are included in this published article and its Supporting Information.

Supporting Information

The Supporting Information is available free of charge at https://pubs.acs.org/doi/10.1021/acsomega.4c05008.

Sequences, binding affinity with K^+, native PAGE analysis, CD spectra and their SVD analyses, and UV melting curves of DNA oligonucleotides used in this study (PDF)

■ AUTHOR INFORMATION

Corresponding Author

Daisuke Miyoshi − *Faculty of Frontiers of Innovative Research in Science and Technology (FIRST), Konan University, Kobe 650-0047, Japan*; orcid.org/0000-0002-4308-0499; Phone: +81-78-303-1426; Email: miyoshi@konan-u.ac.jp; Fax: +81-78-303-1495

Authors

Minori Nakata − *Faculty of Frontiers of Innovative Research in Science and Technology (FIRST), Konan University, Kobe 650-0047, Japan*

Naoki Kosaka − *Faculty of Frontiers of Innovative Research in Science and Technology (FIRST), Konan University, Kobe 650-0047, Japan*

Keiko Kawauchi − *Faculty of Frontiers of Innovative Research in Science and Technology (FIRST), Konan University, Kobe 650-0047, Japan*

Complete contact information is available at: https://pubs.acs.org/10.1021/acsomega.4c05008

Author Contributions

Conceptualization: D.M.; methodology: D.M.; formal analysis: M.N. and N.K.; investigation: M.N. and N.K.; data curation: M.N.; writing of the original draft: M.N.; review and editing: K.K. and D.M.; visualization: D.M.; supervision: K.K. and D.M.; project administration: D.M.; funding acquisition: D.M. and K.K.

Notes

The authors declare no competing financial interest.

■ ACKNOWLEDGMENTS

This work was supported by JSPS KAKENHI grant numbers 24K21801, 23H03020, 21H02062, 20K21259, and 17H06351, Research Grants from the Asahi Glass Foundation, Japan, the Junzo Tateno Foundation, and the Hirao Taro Foundation of Konan Gakuen for Academic Research, Japan.

■ REFERENCES

(1) Smith, F. W.; Feigon, J. Quadruplex structure of Oxytricha telomeric DNA oligonucleotides. *Nature* **1992**, *356* (6365), 164−8.

(2) Sen, D.; Gilbert, W. Formation of parallel four-stranded complexes by guanine-rich motifs in DNA and its implications for meiosis. *Nature* **1988**, *334* (6180), 364−6.

(3) Agrawal, P.; Lin, C.; Mathad, R. I.; Carver, M.; Yang, D. The major G-quadruplex formed in the human BCL-2 proximal promoter adopts a parallel structure with a 13-nt loop in K+ solution. *J. Am. Chem. Soc.* **2014**, *136* (5), 1750−3.

(4) Chaudhuri, R.; Bhattacharya, S.; Dash, J.; Bhattacharya, S. Recent Update on Targeting c-MYC G-Quadruplexes by Small Molecules for Anticancer Therapeutics. *J. Med. Chem.* **2021**, *64* (1), 42−70.

(5) Parkinson, G. N.; Lee, M. P.; Neidle, S. Crystal structure of parallel quadruplexes from human telomeric DNA. *Nature* **2002**, *417* (6891), 876−80.

(6) Spiegel, J.; Adhikari, S.; Balasubramanian, S. The Structure and Function of DNA G-Quadruplexes. *Trends Chem.* **2020**, *2* (2), 123−136.

(7) Varshney, D.; Spiegel, J.; Zyner, K.; Tannahill, D.; Balasubramanian, S. The regulation and functions of DNA and RNA G-quadruplexes. *Nat. Rev. Mol. Cell Biol.* **2020**, *21* (8), 459−474.

(8) Rhodes, D.; Lipps, H. J. G-quadruplexes and their regulatory roles in biology. *Nucleic Acids Res.* **2015**, *43* (18), 8627−37.

(9) Zahler, A. M.; Williamson, J. R.; Cech, T. R.; Prescott, D. M. Inhibition of telomerase by G-quartet DNA structures. *Nature* **1991**, *350* (6320), 718−20.
(10) Valton, A. L.; Hassan-Zadeh, V.; Lema, I.; Boggetto, N.; Alberti, P.; Saintome, C.; Riou, J. F.; Prioleau, M. N. G4 motifs affect origin positioning and efficiency in two vertebrate replicators. *EMBO. J.* **2014**, *33* (7), 732−46.
(11) Siddiqui-Jain, A.; Grand, C. L.; Bearss, D. J.; Hurley, L. H. Direct evidence for a G-quadruplex in a promoter region and its targeting with a small molecule to repress c-MYC transcription. *Proc. Natl. Acad. Sci. U. S. A.* **2002**, *99* (18), 11593−8.
(12) Thakur, R. K.; Kumar, P.; Halder, K.; Verma, A.; Kar, A.; Parent, J. L.; Basundra, R.; Kumar, A.; Chowdhury, S. Metastases suppressor NM23-H2 interaction with G-quadruplex DNA within c-MYC promoter nuclease hypersensitive element induces c-MYC expression. *Nucleic Acids Res.* **2009**, *37* (1), 172−83.
(13) Cebrian, R.; Belmonte-Reche, E.; Pirota, V.; de Jong, A.; Morales, J. C.; Freccero, M.; Doria, F.; Kuipers, O. P. G-Quadruplex DNA as a Target in Pathogenic Bacteria: Efficacy of an Extended Naphthalene Diimide Ligand and Its Mode of Action. *J. Med. Chem.* **2022**, *65* (6), 4752−4766.
(14) Moye, A. L.; Porter, K. C.; Cohen, S. B.; Phan, T.; Zyner, K. G.; Sasaki, N.; Lovrecz, G. O.; Beck, J. L.; Bryan, T. M. Telomeric G-quadruplexes are a substrate and site of localization for human telomerase. *Nat. Commun.* **2015**, *6*, 7643.
(15) Vannier, J. B.; Pavicic-Kaltenbrunner, V.; Petalcorin, M. I.; Ding, H.; Boulton, S. J. RTEL1 dismantles T loops and counteracts telomeric G4-DNA to maintain telomere integrity. *Cell* **2012**, *149* (4), 795−806.
(16) Monsen, R. C.; Maguire, J. M.; DeLeeuw, L. W.; Chaires, J. B.; Trent, J. O. Drug discovery of small molecules targeting the higher-order hTERT promoter G-quadruplex. *PLoS One* **2022**, *17* (6), No. e0270165.
(17) Seimiya, H.; Nagasawa, K.; Shin-Ya, K. Chemical targeting of G-quadruplexes in telomeres and beyond for molecular cancer therapeutics. *J. Antibiot. (Tokyo)* **2021**, *74* (10), 617−628.
(18) Asamitsu, S.; Yabuki, Y.; Ikenoshita, S.; Kawakubo, K.; Kawasaki, M.; Usuki, S.; Nakayama, Y.; Adachi, K.; Kugoh, H.; Ishii, K.; Matsuura, T.; Nanba, E.; Sugiyama, H.; Fukunaga, K.; Shioda, N. CGG repeat RNA G-quadruplexes interact with FMRpolyG to cause neuronal dysfunction in fragile X-related tremor/ataxia syndrome. *Sci. Adv.* **2021**, *7* (3), No. eabd9440.
(19) Qin, G.; Zhao, C.; Liu, Y.; Zhang, C.; Yang, G.; Yang, J.; Wang, Z.; Wang, C.; Tu, C.; Guo, Z.; Ren, J.; Qu, X. RNA G-quadruplex formed in SARS-CoV-2 used for COVID-19 treatment in animal models. *Cell Discovery* **2022**, *8* (1), 86.
(20) Sugimoto, W.; Kinoshita, N.; Nakata, M.; Ohyama, T.; Tateishi-Karimata, H.; Nishikata, T.; Sugimoto, N.; Miyoshi, D.; Kawauchi, K. Intramolecular G-quadruplex-hairpin loop structure competition of a GC-rich exon region in the TMPRSS2 gene. *Chem. Commun. (Camb)* **2021**, *58* (1), 48−51.
(21) Tateishi-Karimata, H.; Isono, N.; Sugimoto, N. New insights into transcription fidelity: thermal stability of non-canonical structures in template DNA regulates transcriptional arrest, pause, and slippage. *PLoS One* **2014**, *9* (3), No. e90580.
(22) Bhattacharyya, D.; Mirihana Arachchilage, G.; Basu, S. Metal Cations in G-Quadruplex Folding and Stability. *Front. Chem.* **2016**, *4*, 38.
(23) Chen, F. M. Sr2+ facilitates intermolecular G-quadruplex formation of telomeric sequences. *Biochemistry* **1992**, *31* (15), 3769−76.
(24) Guedin, A.; Gros, J.; Alberti, P.; Mergny, J. L. How long is too long? Effects of loop size on G-quadruplex stability. *Nucleic Acids Res.* **2010**, *38* (21), 7858−68.
(25) Largy, E.; Mergny, J. L.; Gabelica, V. Role of Alkali Metal Ions in G-Quadruplex Nucleic Acid Structure and Stability. *Met. Ions Life Sci.* **2016**, *16*, 203−58.
(26) Miyoshi, D.; Karimata, H.; Sugimoto, N. Hydration regulates thermodynamics of G-quadruplex formation under molecular crowding conditions. *J. Am. Chem. Soc.* **2006**, *128* (24), 7957−63.
(27) Kankia, B. I.; Marky, L. A. Folding of the thrombin aptamer into a G-quadruplex with Sr(2+): stability, heat, and hydration. *J. Am. Chem. Soc.* **2001**, *123* (44), 10799−804.
(28) Zaccaria, F.; Paragi, G.; Fonseca Guerra, C. The role of alkali metal cations in the stabilization of guanine quadruplexes: why K(+) is the best. *Phys. Chem. Chem. Phys.* **2016**, *18* (31), 20895−904.
(29) Zhu, H.; Xiao, S.; Wang, L.; Liang, H. Communication: Asymmetrical cation movements through G-quadruplex DNA. *J. Chem. Phys.* **2014**, *141* (4), No. 041103.
(30) Oganesian, L.; Moon, I. K.; Bryan, T. M.; Jarstfer, M. B. Extension of G-quadruplex DNA by ciliate telomerase. *EMBO J.* **2006**, *25* (5), 1148−59.
(31) Zhang, J. y.; Xia, Y.; Hao, Y. h.; Tan, Z. DNA:RNA hybrid G-quadruplex formation upstream of transcription start site. *Sci. Rep.* **2020**, *10* (1), 7429.
(32) Sen, D.; Gilbert, W. A sodium-potassium switch in the formation of four-stranded G4-DNA. *Nature* **1990**, *344* (6265), 410−4.
(33) Cheng, M.; Cheng, Y.; Hao, J.; Jia, G.; Zhou, J.; Mergny, J. L.; Li, C. Loop permutation affects the topology and stability of G-quadruplexes. *Nucleic Acids Res.* **2018**, *46* (18), 9264−9275.
(34) Lim, K. W.; Phan, A. T. Structural basis of DNA quadruplex-duplex junction formation. *Angew. Chem., Int. Ed. Engl.* **2013**, *52* (33), 8566−9.
(35) Lim, K. W.; Khong, Z. J.; Phan, A. T. Thermal stability of DNA quadruplex-duplex hybrids. *Biochemistry* **2014**, *53* (1), 247−57.
(36) Nguyen, T. Q. N.; Lim, K. W.; Phan, A. T. Folding Kinetics of G-Quadruplexes: Duplex Stem Loops Drive and Accelerate G-Quadruplex Folding. *J. Phys. Chem. B* **2020**, *124* (25), 5122−5130.
(37) Vianney, Y. M.; Weisz, K. Indoloquinoline Ligands Favor Intercalation at Quadruplex-Duplex Interfaces. *Chemistry* **2022**, *28* (7), No. e202103718.
(38) Phan, A. T.; Kuryavyi, V.; Darnell, J. C.; Serganov, A.; Majumdar, A.; Ilin, S.; Raslin, T.; Polonskaia, A.; Chen, C.; Clain, D.; Darnell, R. B.; Patel, D. J. Structure-function studies of FMRP RGG peptide recognition of an RNA duplex-quadruplex junction. *Nat. Struct. Mol. Biol.* **2011**, *18* (7), 796−804.
(39) Vasilyev, N.; Polonskaia, A.; Darnell, J. C.; Darnell, R. B.; Patel, D. J.; Serganov, A. Crystal structure reveals specific recognition of a G-quadruplex RNA by a beta-turn in the RGG motif of FMRP. *Proc. Natl. Acad. Sci. U. S. A.* **2015**, *112* (39), E5391−E5400.
(40) Podbevsek, P.; Hud, N. V.; Plavec, J. NMR evaluation of ammonium ion movement within a unimolecular G-quadruplex in solution. *Nucleic Acids Res.* **2007**, *35* (8), 2554−63.
(41) Mullen, M. A.; Assmann, S. M.; Bevilacqua, P. C. Toward a digital gene response: RNA G-quadruplexes with fewer quartets fold with higher cooperativity. *J. Am. Chem. Soc.* **2012**, *134* (2), 812−5.
(42) Tan, D. J. Y.; Winnerdy, F. R.; Lim, K. W.; Phan, A. T. Coexistence of two quadruplex-duplex hybrids in the PIM1 gene. *Nucleic Acids Res.* **2020**, *48* (19), 11162−11171.
(43) Horiuchi, D.; Camarda, R.; Zhou, A. Y.; Yau, C.; Momcilovic, O.; Balakrishnan, S.; Corella, A. N.; Eyob, H.; Kessenbrock, K.; Lawson, D. A.; Marsh, L. A.; Anderton, B. N.; Rohrberg, J.; Kunder, R.; Bazarov, A. V.; Yaswen, P.; McManus, M. T.; Rugo, H. S.; Werb, Z.; Goga, A. PIM1 kinase inhibition as a targeted therapy against triple-negative breast tumors with elevated MYC expression. *Nat. Med.* **2016**, *22* (11), 1321−1329.
(44) Brault, L.; Gasser, C.; Bracher, F.; Huber, K.; Knapp, S.; Schwaller, J. PIM serine/threonine kinases in the pathogenesis and therapy of hematologic malignancies and solid cancers. *Haematologica.* **2010**, *95* (6), 1004−15.
(45) Chen, W. W.; Chan, D. C.; Donald, C.; Lilly, M. B.; Kraft, A. S. Pim family kinases enhance tumor growth of prostate cancer cells. *Mol. Cancer Res.* **2005**, *3* (8), 443−51.

https://doi.org/10.1021/acsomega.4c05008
ACS Omega 2024, 9, 35028−35036

(46) Del Villar-Guerra, R.; Trent, J. O.; Chaires, J. B. G-Quadruplex Secondary Structure Obtained from Circular Dichroism Spectroscopy. *Angew. Chem., Int. Ed. Engl.* **2018**, *57* (24), 7171−7175.
(47) Carrera, P.; Azorin, F. Structural characterization of intrinsically curved AT-rich DNA sequences. *Nucleic Acids Res.* **1994**, *22* (18), 3671−80.
(48) Stellwagen, N. C. Electrophoresis of DNA in agarose gels, polyacrylamide gels and in free solution. *Electrophoresis* **2009**, *30 Suppl. 1* (Suppl 1), S188−S195.
(49) Napolitano, E.; Criscuolo, A.; Riccardi, C.; Esposito, C. L.; Catuogno, S.; Coppola, G.; Roviello, G. N.; Montesarchio, D.; Musumeci, D. Directing in Vitro Selection towards G-quadruplex-forming Aptamers to Inhibit HMGB1 Pathological Activity. *Angew. Chem., Int. Ed. Engl.* **2024**, *63* (16), No. e202319828.
(50) Miyoshi, D.; Nakao, A.; Sugimoto, N. Structural transition from antiparallel to parallel G-quadruplex of d(G4T4G4) induced by Ca2+. *Nucleic Acids Res.* **2003**, *31* (4), 1156−63.
(51) Yu, Z.; Gaerig, V.; Cui, Y.; Kang, H.; Gokhale, V.; Zhao, Y.; Hurley, L. H.; Mao, H. Tertiary DNA structure in the single-stranded hTERT promoter fragment unfolds and refolds by parallel pathways via cooperative or sequential events. *J. Am. Chem. Soc.* **2012**, *134* (11), 5157−64.
(52) Mashimo, T.; Yagi, H.; Sannohe, Y.; Rajendran, A.; Sugiyama, H. Folding pathways of human telomeric type-1 and type-2 G-quadruplex structures. *J. Am. Chem. Soc.* **2010**, *132* (42), 14910−8.
(53) Gray, R. D.; Trent, J. O.; Chaires, J. B. Folding and unfolding pathways of the human telomeric G-quadruplex. *J. Mol. Biol.* **2014**, *426* (8), 1629−50.
(54) Mergny, J. L.; Phan, A. T.; Lacroix, L. Following G-quartet formation by UV-spectroscopy. *FEBS Lett.* **1998**, *435* (1), 74−8.
(55) Yu, H.; Gu, X.; Nakano, S.; Miyoshi, D.; Sugimoto, N. Beads-on-a-string structure of long telomeric DNAs under molecular crowding conditions. *J. Am. Chem. Soc.* **2012**, *134* (49), 20060−9.
(56) Serra, M. J.; Lyttle, M. H.; Axenson, T. J.; Schadt, C. A.; Turner, D. H. RNA hairpin loop stability depends on closing base pair. *Nucleic Acids Res.* **1993**, *21* (16), 3845−9.
(57) Moody, E. M.; Bevilacqua, P. C. Thermodynamic coupling of the loop and stem in unusually stable DNA hairpins closed by CG base pairs. *J. Am. Chem. Soc.* **2003**, *125* (8), 2032−3.
(58) Kannan, S.; Zacharias, M. Role of the closing base pair for d(GCA) hairpin stability: free energy analysis and folding simulations. *Nucleic Acids Res.* **2011**, *39* (19), 8271−80.
(59) Hilbers, C. W.; Haasnoot, C. A.; de Bruin, S. H.; Joordens, J. J.; van der Marel, G. A.; van Boom, J. H. Hairpin formation in synthetic oligonucleotides. *Biochimie.* **1985**, *67* (7−8), 685−95.
(60) Senior, M. M.; Jones, R. A.; Breslauer, K. J. Influence of loop residues on the relative stabilities of DNA hairpin structures. *Proc. Natl. Acad. Sci. U. S. A.* **1988**, *85* (17), 6242−6.
(61) Zuker, M. Mfold web server for nucleic acid folding and hybridization prediction. *Nucleic Acids Res.* **2003**, *31* (13), 3406−15.
(62) Hazel, P.; Huppert, J.; Balasubramanian, S.; Neidle, S. Loop-length-dependent folding of G-quadruplexes. *J. Am. Chem. Soc.* **2004**, *126* (50), 16405−15.
(63) Bugaut, A.; Balasubramanian, S. A sequence-independent study of the influence of short loop lengths on the stability and topology of intramolecular DNA G-quadruplexes. *Biochemistry* **2008**, *47* (2), 689−97.
(64) Sugimoto, N.; Nakano, M.; Nakano, S. Thermodynamics-structure relationship of single mismatches in RNA/DNA duplexes. *Biochemistry* **2000**, *39* (37), 11270−81.
(65) Compton, L. A.; Johnson, W. C., Jr. Analysis of protein circular dichroism spectra for secondary structure using a simple matrix multiplication. *Anal. Biochem.* **1986**, *155* (1), 155−67.
(66) Johnson, K. A. Fitting enzyme kinetic data with KinTek Global Kinetic Explorer. *Methods Enzymol.* **2009**, *467*, 601−626.
(67) Fang, X.; Pan, T.; Sosnick, T. R. A thermodynamic framework and cooperativity in the tertiary folding of a Mg2+-dependent ribozyme. *Biochemistry* **1999**, *38* (51), 16840−6.
(68) Goutelle, S.; Maurin, M.; Rougier, F.; Barbaut, X.; Bourguignon, L.; Ducher, M.; Maire, P. The Hill equation: a review of its capabilities in pharmacological modelling. *Fundam. Clin. Pharmacol.* **2008**, *22* (6), 633−48.
(69) Nakano, S.; Fujimoto, M.; Hara, H.; Sugimoto, N. Nucleic acid duplex stability: influence of base composition on cation effects. *Nucleic Acids Res.* **1999**, *27* (14), 2957−65.
(70) Sugimoto, N.; Nakano, S.; Katoh, M.; Matsumura, A.; Nakamuta, H.; Ohmichi, T.; Yoneyama, M.; Sasaki, M. Thermodynamic parameters to predict stability of RNA/DNA hybrid duplexes. *Biochemistry* **1995**, *34* (35), 11211−6.

https://doi.org/10.1021/acsomega.4c05008
ACS Omega 2024, 9, 35028−35036